A HIGHLY PARALLEL MULTILEVEL NEWTON-KRYLOV-SCHWARZ METHOD WITH SUBSPACE-BASED COARSENING AND PARTITION-BASED BALANCING FOR THE MULTIGROUP NEUTRON TRANSPORT EQUATIONS ON 3D UNSTRUCTURED MESHES

FANDE KONG*†, YAQI WANG ‡, DEREK R. GASTON†, CODY J. PERMANN†, ANDREW E. SLAUGHTER†, ALEXANDER D. LINDSAY†, AND RICHARD C. MARTINEAU†

Abstract. The multigroup neutron transport equations have been widely used to study the motion of neutrons and their interactions with the background materials. Numerical simulation of the multigroup neutron transport equations is computationally challenging because the equations is defined on a high dimensional phase space (1D in energy, 2D in angle, and 3D in spatial space), and furthermore, for realistic applications, the computational spatial domain is complex and the materials are heterogeneous. The multilevel domain decomposition methods is one of the most popular algorithms for solving the multigroup neutron transport equations, but the construction of coarse spaces is expensive and often not strongly scalable when the number of processor cores is large. A scalable algorithm has to be designed in such a way that the compute time is almost halved without any comprise on the solution accuracy when the number of processor cores is doubled. In this paper, we study a highly parallel multilevel Newton-Krylov-Schwarz method equipped with several novel components, such as subspace-based coarsening, partition-based balancing and hierarchical mesh partitioning, that enable the overall simulation strongly scalable in terms of the compute time. Compared with the traditional coarsening method, the subspace-based coarsening algorithm significantly reduces the cost of the preconditioner setup that is often unscalable. In addition, the partition-based balancing strategy enhances the parallel efficiency of the overall solver by assigning a nearly-equal amount of work to each processor core. The hierarchical mesh partitioning is able to generate a large number of subdomains and meanwhile minimizes the off-node communication. We numerically show that the proposed algorithm is scalable with more than 10,000 processor cores for a realistic application with a few billions unknowns on 3D unstructured meshes.

Key words. Neutron transport equations, Newton-Krylov-Schwarz, mesh partitioning, workload balancing, parallel computation, multilevel domain decomposition methods

AMS subject classifications. 65N55, 65Y05, 65N25, 65N30

1. Introduction. The multigroup neutron transport equations is employed to describe the motion of neutrons and their interactions with the background materials [21]. The fundamental quantity of interest is the statistically averaged neutron distribution, referred to as "flux", in a high dimensional phase space (1D in energy, 2D in angle, 3D in space). We consider the time-independent version of the equations here so that the time dimension is not taken into account. The neutron flux is a scalar quantity physically representing the total length traveled by all free neutrons per unit time and volume. For solving the neutron transport equations, some fundamental nuclear data (referred to as "cross sections") describing the likelihood per unit path length of neutrons interacting with the background materials is required. The cross sections depend on the energy and temperature of the background materials in a complicated manner [21]. The neutron transport equations can behavior as hyperbolic and elliptic forms under simple changes in cross sections (material properties) that may occur in realistic applications [10]. Because of the large dimensionality, the complicated solution behaviors, the complex computational domain and the heterogeneous materials, the neutron simulations are among the most memory and computation intensive in all of computational science. Therefore, a scalable parallel solution

^{*}Corresponding Author: fande.kong@inl.gov

[†]Computational Frameworks, Idaho National Laboratory, Idaho Falls, ID 83415

[‡]Nuclear Engineering Methods Development, Idaho National Laboratory, Idaho Falls, ID 83415

approach that takes advantages of modern supercomputers plays a critical role in the transport simulations. In this paper, we propose a scalable parallel nonoverlapping Newton-Krylov-Schwarz (NKS) method for the high-resolution simulation of the multigroup neutron transport equations. The performance of NKS is almost completely determined by the preconditioner. To achieve a high-performance neutron simulation, we develop a multilevel domain decomposition method with including a novel subspace-based coarsening scheme, a partition-based balancing strategy and a hierarchical mesh partitioning approach.

The development of efficient algorithms for the neutron simulations has been an active research topic for a couple of decades, and many solvers were studied. Multilevel domain decomposition and algebraic multigrid (AMG) methods are ones of the most popular algorithms for the numerical solution of the neutron transport equations. We briefly review the multilevel and AMG methods here, and for other popular methods such as the transport sweeps, interested readers are referred to [21, 35]. With the development of supercomputers, the domains decomposition methods become attractive because they are naturally suitable for parallel computations. In [31], the second-order even-parity form of the time-independent Boltzaman transport equations is solved with fGMRES preconditioned by an one-level overlapping domain decomposition method, where ILU together with CG is chosen as a local subdomain solver. The algorithm is numerically demonstrated to scale up to a few hundreds processor cores, but the scalability drops significantly when using 1,000 processor cores. In [8], a nonoverlapping domain decomposition with Robin interface conditions is studied for the simplified transport approximation, and the parallel efficiency is reported using up to 25 processors cores. In [10], the parallel computation is implemented using a space-angle-group decomposition method, where the "within-group" equation is solved using a Richardson iteration. A two-level overlapping Schwarz preconditioner is developed for the multigroup neutron diffusions equations in [19].

The algebraic multigrid (AMG) methods can be implemented in space, angle or energy. A spatial multigrid algorithm is presented for the isotropic neutron transport equations with a simple 2D geometry in [4], where the algorithm works well for homogeneous domains but the convergence need to be improved for heterogeneous domains. In [30], an angular multgrid method is used as a preconditioner for the GMRES method for the problems with highly forward-peaked scattering, and the method is numerically shown to be more efficient than an analogous DSA-preconditioned (diffusion synthetic acceleration [1]) Krylov subspace method. A multigrid-in-energy preconditioner (MGE) together with a Krylov subspace solver is proposed in [26]. The MGE preconditioner reduces the number of Krylov iterations in both the fixed source and eigenvalue problems.

The multilevel and AMG methods are used for a wide range of problems in the neutron transport, but the construction of coarse spaces is challenging and often unscalable when the number of processor cores becomes large. To have scalable simulations, we take an attempt to address these issues using the NKS method equipped with two important ingredients, subspace-based coarsening and partitioned-based balancing. In this paper, the multigroup transport equations is discretized in space using the first order continuous finite element method and in angle using the discrete ordinates approach. The resulting algebraic system of equations is solved with Jacobian-free Newton-Krylov (PJFNK) [11], where the preconditioning matrix is formed with the streaming and collision operator. During each Newton iteration, the Jacobian system is calculated by a Krylov subspace method such as GMRES precondi-

tioned by a multilevel nonverlapping Schwarz. The coarse spaces can be constructed either geometrically or algebraically. In our previous works [13, 14, 15], some boundary preserving coarse spaces are constructed geometrically, and they are shown to work well for elasticity problems and fluid-structure interaction problems. Unfortunately, the geometric coarsening method is unavailable for the targeting application since the computational domain, shown in Fig. 1, used in this work includes many different regions that are meshed using different element types. Instead, an algebraic coarsening algorithm is employed to construct coarse spaces for the multilevel Schwarz method. However, if the traditional coarsening method is employed, the overall algorithm performance will be deteriorated and the strong scalability can not be maintained. To overcome the difficulty, we introduce a novel subspace-based coarsening algorithm that reduces the preconditionr setup time significantly compared with the traditional coarsening method, which makes the overall algorithm scalable with more than 10,000 processor cores. In addition, a partition-based balancing scheme is included to enhance the parallel efficiency, and a hierarchical mesh partitioning approach is studied to generate a large number of subdomains.

The rest of this paper is organized as follows. In Section 2, the multigroup neutron transport equations and its spatial and angular discretizations are described in detail. And a highly parallel Newton-Krylov-Schwarz framework is presented in Section 3. A novel subspace-based coarsening algorithm is introduced, in Section 4, to construct coarse spaces for building an efficient Schwarz preconditioner. In Section 5, some numerical tests are carefully studied to demonstrate the performance of the proposed algorithm. A few remarks and conclusions are drawn in Section 6.

- **2. Problem description.** In this section, we first describe the multigroup neutron transport equations in detail, and then present the corresponding spatial and angular discretizations.
- **2.1. Multigroup neutron transport equations.** The fundamental quantity of interest, neutron angular flux Ψ_g [cm⁻² s⁻¹ st⁻¹], is governed by the multigroup neutron transport equations in $\mathcal{D} \times \mathcal{S}$ as follows:

(2.1a)
$$\begin{split} \vec{\Omega} \cdot \vec{\nabla} \Psi_{g} + \Sigma_{t,g} \Psi_{g} &= \sum_{g'=1}^{G} \int_{\mathcal{S}} \Sigma_{s,g' \to g} f_{g' \to g} (\vec{\Omega}' \cdot \vec{\Omega}) \Psi_{g'} (\vec{x}, \vec{\Omega}') \, d\Omega' \\ &+ \frac{1}{4\pi} \frac{\chi_{g}}{k} \sum_{g'=1}^{G} \nu \Sigma_{f,g'} \Phi_{g'}, \text{ in } \mathcal{D} \times \mathcal{S}, \end{split}$$

$$(2.1b) \qquad \Psi_g = \alpha_g^s \Psi_g(\vec{\Omega}_r) + \alpha_g^d \frac{\int_{\vec{\Omega}' \cdot \vec{n}_b > 0} \left| \vec{\Omega}' \cdot \vec{n}_b \right| \Psi_g d\Omega'}{\int_{\vec{\Omega}' \cdot \vec{n}_b > 0} \left| \vec{\Omega}' \cdot \vec{n}_b \right| d\Omega'}, \text{ on } \partial \mathcal{D} : \vec{\Omega} \cdot \vec{n}_b < 0,$$

where $g=1,\cdots,G$, and G is the number of energy groups. \mathcal{D} is a 3D spatial domain (e.g, shown in Fig. 1) and S is a 2D sphere. $\vec{x}\in\mathcal{D}$ is the independent spatial variable $[\operatorname{cm}]$, $\vec{\Omega}\in S$ denotes the independent angular variable, $\vec{\Omega}_r=\vec{\Omega}-2(\vec{\Omega}\cdot\vec{n}_b)\vec{n}_b$, $\partial\mathcal{D}$ is the boundary of \mathcal{D} , \vec{n}_b is the outward unit normal vector on the boundary, $\Sigma_{t,g}$ is the macroscopic total cross section $[\operatorname{cm}^{-1}]$, $\Sigma_{s,g'\to g}$ is the macroscopic scattering cross section from group g' to group $g[\operatorname{cm}^{-1}]$, α_g^s is the specular reflectivity on $\partial\mathcal{D}$, α_g^d is the diffusive reflectivity on $\partial\mathcal{D}$, k is the eigenvalue (sometimes referred to as

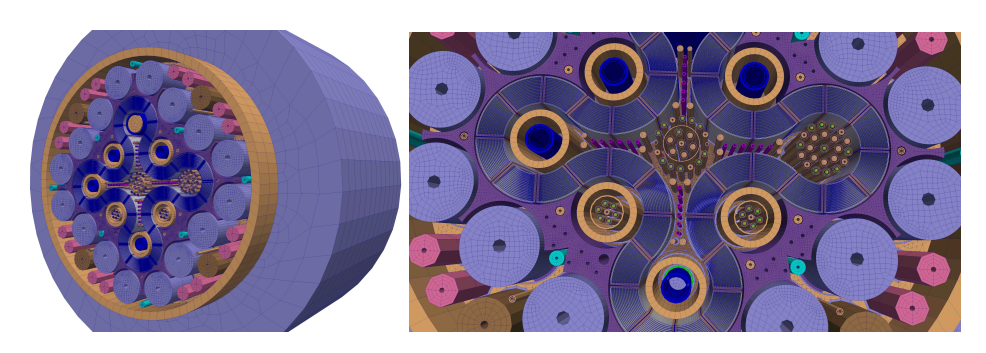


FIG. 1. 3D unstructured mesh. Right: zoom-in picture of the top mesh. Different colors correspond to different materials.

a multiplication factor), χ_g is the prompt fission spectrum, $\Sigma_{f,g}$ is the macroscopic fission cross section $[\operatorname{cm}^{-1}]$, and ν is the averaged neutron emitted per fission. Φ_g is the scalar flux $[\operatorname{cm}^{-2}\operatorname{s}^{-1}]$ defined as $\Phi_g \equiv \int_{\mathcal{S}} \Psi_g \, d\Omega$, and $f_{g'\to g}$ is the scattering phase function. In (2.1a), the first term is the *streaming term*, and the second is the *collision* term. The first term of (2.1a) on the right hand side is the *scattering term*, which couples the angular fluxes of all directions and energy groups together. The second term of the right hand side of (2.1a) is the fission term, which also couples the angular fluxes of all directions and energy groups together. For a more detailed description on the neutron transport equations, please see [21, 33].

For convenience, let us define some operators:

$$\begin{split} \mathbf{L}\mathbf{\Psi} &\equiv \left[\mathbb{L}_{1}\Psi_{1},\mathbb{L}_{2}\Psi_{2},\cdots,\mathbb{L}_{G}\Psi_{G}\right]^{T},\ \mathbb{L}_{g}\Psi_{g} \equiv \vec{\nabla}\cdot\vec{\Omega}\Psi_{g} + \Sigma_{\mathbf{t},g}\Psi_{g},\\ \mathbf{S}\mathbf{\Psi} &\equiv \left[\mathbb{S}_{1}\Psi_{1},\mathbb{S}_{2}\Psi_{2},\cdots,\mathbb{S}_{G}\Psi_{G}\right]^{T},\ \mathbb{S}_{g}\Psi_{g} \equiv \sum_{g'=1}^{G}\int_{\mathcal{S}}\Sigma_{\mathbf{s},g'\to g}f_{g'\to g}\Psi_{g'}\,d\Omega',\\ \mathbf{F}\mathbf{\Psi} &\equiv \left[\mathbb{F}_{1}\Psi_{1},\mathbb{F}_{2}\Psi_{2},\cdots,\mathbb{F}_{G}\Psi_{G}\right]^{T},\ \mathbb{F}_{g}\Psi_{g} \equiv \frac{1}{4\pi}\chi_{g}\sum_{g'=1}^{G}\nu\Sigma_{\mathbf{f},g'}\Phi_{g'}. \end{split}$$

Here **L** is the streaming-collision operator, **S** is the scattering operator and **F** is the fission operator. Similarly, the operator for the boundary condition mapping from $\partial \mathcal{D} \times \mathcal{S}_{\vec{n}_h}^+$ to $\partial \mathcal{D} \times \mathcal{S}_{\vec{n}_h}^-$ is defined as

$$\mathbf{B}\mathbf{\Psi} \equiv \left[\mathbb{B}_{1}\Psi_{1}, \mathbb{B}_{2}\Psi_{2}, \cdots, \mathbb{B}_{G}\Psi_{G}\right]^{T}, \ \mathbb{B}_{g}\Psi_{g} \equiv \alpha_{g}^{s}\Psi_{g}(\vec{\Omega}_{r}) + \alpha_{g}^{d} \frac{\int_{\vec{\Omega}' \cdot \vec{n}_{b} > 0} \left|\vec{\Omega}' \cdot \vec{n}_{b}\right| \Psi_{g}(\vec{\Omega}') d\Omega'}{\int_{\vec{\Omega}' \cdot \vec{n}_{b} > 0} \left|\vec{\Omega}' \cdot \vec{n}_{b}\right| d\Omega'}.$$

where $\mathcal{S}_{\vec{n}_b}^{\pm} = \left\{ \vec{\Omega} \in \mathcal{S}, \vec{\Omega} \cdot \vec{n}_b \geqslant 0 \right\}$ is a half angular space defined with respect to the unit vector \vec{n}_b . Finally, (2.1a) is rewritten as

(2.2)
$$\mathbf{L}\Psi = \mathbf{S}\Psi + \frac{1}{k}\mathbf{F}\Psi,$$

with the boundary condition $\Psi = \mathbf{B}\Psi$ corresponding to (2.1b).

2.2. Spatial and angular discretizations. Before the weak form of (2.2) is presented, some notations are introduced. An inner product is defined as

$$(\mathbf{a}, \mathbf{b})_{\mathcal{D} \times \mathcal{S}} \equiv \sum_{g=1}^{G} \int_{\mathcal{S}} d\Omega \int_{\mathcal{D}} dx \, a_{g}(\vec{x}, \vec{\Omega}) b_{g}(\vec{x}, \vec{\Omega}),$$

where **a** and **b** are generic multigroup functions defined in $\mathcal{D} \times \mathcal{S}$. We drop the subscript $\mathcal{D} \times \mathcal{S}$ for notation simplicity. We also have a similar definition for the boundary integral as :

$$\langle \mathbf{a}, \mathbf{b} \rangle \equiv \langle \mathbf{a}, \mathbf{b} \rangle^+ + \langle \mathbf{a}, \mathbf{b} \rangle^-, \ \langle \mathbf{a}, \mathbf{b} \rangle^{\pm} \equiv \sum_{g=1}^G \oint_{\partial \mathcal{D}} dx \int_{\mathcal{S}_{\vec{n}_b}^{\pm}} d\Omega \ \left| \vec{\Omega} \cdot \vec{n}_b \right| a_g(\vec{x}, \vec{\Omega}) b_g(\vec{x}, \vec{\Omega}).$$

Following a standard finite element technique, we multiply a test function Ψ^* with (2.2), and then integrate over the phase space, $\mathcal{D} \times \mathcal{S}$,

(2.3)
$$(\mathbf{\Psi}^*, \mathbf{L}\mathbf{\Psi}) = (\mathbf{\Psi}^*, \mathbf{S}\mathbf{\Psi}) + \frac{1}{k} (\mathbf{\Psi}^*, \mathbf{F}\mathbf{\Psi}).$$

After some manipulations, the weak form reads as

(2.4)
$$(\mathbf{L}^*\mathbf{\Psi}^*,\mathbf{\Psi}) + \langle \mathbf{\Psi}^*,\mathbf{\Psi} \rangle^+ - \langle \mathbf{\Psi}^*,\mathbf{B}\mathbf{\Psi} \rangle^- = (\mathbf{\Psi}^*,\mathbf{S}\mathbf{\Psi}) + \frac{1}{k} (\mathbf{\Psi}^*,\mathbf{F}\mathbf{\Psi}),$$

where L^* is the adjoint operator of L. The form (2.4) is usually unstable, and here a stabilizing technique, SAAF (self-adjoint angular flux), is included to remedy this issue. In the SAAF method, the streaming-collision operator L is split into two parts (the streaming operator L_1 and the collision operator L_2),

$$(2.5) L\Psi \equiv L_1\Psi + L_2\Psi,$$

where

$$\begin{split} \mathbf{L}_{1}\mathbf{\Psi} &\equiv \left[\mathbb{L}_{1,1}\Psi_{1},\mathbb{L}_{1,2}\Psi_{2},\cdots,\mathbb{L}_{1,G}\Psi_{G}\right]^{T},\ \mathbb{L}_{1,g}\Psi_{g} \equiv \vec{\Omega}\cdot\vec{\nabla}\Psi_{g},\\ \mathbf{L}_{2}\mathbf{\Psi} &\equiv \left[\mathbb{L}_{2,1}\Psi_{1},\mathbb{L}_{2,2}\Psi_{2},\cdots,\mathbb{L}_{2,G}\Psi_{G}\right]^{T},\ \mathbb{L}_{2,g}\Psi_{g} \equiv \Sigma_{t,g}\Psi_{g}. \end{split}$$

The "inverse" of L2 is further defined as

$$\mathbf{L}_{2}^{-1}\mathbf{\Psi} \equiv \left[\mathbb{L}_{2,1}^{-1}\Psi_{1},\mathbb{L}_{2,2}^{-1}\Psi_{2},\cdots,\mathbb{L}_{2,G}^{-1}\Psi_{G}\right]^{T},\ \mathbb{L}_{2,g}^{-1}\Psi_{g} = \Psi_{g}/\Sigma_{t,g}.$$

It is easy to verify that $L_2^{-1}L_2=I$, $L_2^*=L_2$, $L_1^*=-L_1$ and $L_1L_2=L_2L_1$. With rearranging (2.2), we have

(2.6)
$$\mathbf{\Psi} = \mathbf{L}_2^{-1} \left(\frac{1}{k} \mathbf{F} \mathbf{\Psi} + \mathbf{S} \mathbf{\Psi} - \mathbf{L}_1 \mathbf{\Psi} \right),$$

which is called the *angular flux equation* (AFE). We substitute (2.6) into the streaming kernel of (2.4),

$$\overline{\left(\mathbf{L}_{1}^{*}\mathbf{\Psi}^{*},\mathbf{\Psi}
ight)} + \left(\mathbf{L}_{2}^{*}\mathbf{\Psi}^{*},\mathbf{\Psi}
ight) + \left\langle \mathbf{\Psi}^{*},\mathbf{\Psi}
ight
angle^{+} - \left\langle \mathbf{\Psi}^{*},\mathbf{B}\mathbf{\Psi}
ight
angle^{-} = \left(\mathbf{\Psi}^{*},\mathbf{S}\mathbf{\Psi}
ight) + \frac{1}{k} \left(\mathbf{\Psi}^{*},\mathbf{F}\mathbf{\Psi}
ight)$$

and obtain the following form after a few manipulations

$$\begin{split} \boxed{ \left(\mathbf{L}_{1}\mathbf{\Psi}^{*}, \mathbf{L}_{2}^{-1}\mathbf{L}_{1}\mathbf{\Psi}\right) + \left(\mathbf{L}_{2}^{*}\mathbf{\Psi}^{*}, \mathbf{\Psi}\right) + \left\langle\mathbf{\Psi}^{*}, \mathbf{\Psi}\right\rangle^{+} } - \left\langle\mathbf{\Psi}^{*}, \mathbf{B}\mathbf{\Psi}\right\rangle^{-} \\ = \left(\mathbf{L}_{2}^{-1}\mathbf{L}\mathbf{\Psi}^{*}, \mathbf{S}\mathbf{\Psi}\right) + \frac{1}{k}\left(\mathbf{L}_{2}^{-1}\mathbf{L}\mathbf{\Psi}^{*}, \mathbf{F}\mathbf{\Psi}\right). \end{split}$$

We noticed that the boxed kernels are symmetric positive definite (SPD), and the calculation of the SPD system is possible using the multilevel method equipped with algebraic coarse spaces. SAAF is equivalent to SUPG (Streamline upwind/Petrov-Galerkin) [3] with the inverse of group-wise total cross sections as the stabilization parameter. Finally, we denote the weak form obtained using the SAAF method as

(2.7)
$$\mathbf{a}\left(\mathbf{\Psi}^{*},\mathbf{\Psi}\right)=\frac{1}{k}\mathbb{f}\left(\mathbf{\Psi}^{*},\mathbf{\Psi}\right),$$

with

$$\begin{split} \mathbf{a}\left(\boldsymbol{\Psi}^{*},\boldsymbol{\Psi}\right) &\equiv \left(\boldsymbol{L}_{1}\boldsymbol{\Psi}^{*},\boldsymbol{L}_{2}^{-1}\boldsymbol{L}_{1}\boldsymbol{\Psi}\right) + \left(\boldsymbol{L}_{2}\boldsymbol{\Psi}^{*},\boldsymbol{\Psi}\right) + \left\langle\boldsymbol{\Psi}^{*},\boldsymbol{\Psi}\right\rangle^{+} \\ &- \left(\boldsymbol{L}_{2}^{-1}\boldsymbol{L}\boldsymbol{\Psi}^{*},\boldsymbol{S}\boldsymbol{\Psi}\right) - \left\langle\boldsymbol{\Psi}^{*},\boldsymbol{B}\boldsymbol{\Psi}\right\rangle^{-}, \\ \mathbf{f}\left(\boldsymbol{\Psi}^{*},\boldsymbol{\Psi}\right) &\equiv \left(\boldsymbol{L}_{2}^{-1}\boldsymbol{L}\boldsymbol{\Psi}^{*},\boldsymbol{F}\boldsymbol{\Psi}\right). \end{split}$$

The S_N (discrete ordinates) method that can be thought of as a collocation method is considered for the angular discretization. Given an angular quadrature set $\left\{\vec{\Omega}_d, w_d, d=1, \cdots, N_d\right\}$ consisting of N_d directions $\vec{\Omega}_d$ and weights w_d , the multigroup transport equations is solved along these directions and all angular integrations in the kernels are numerically evaluated with the angular quadrature. With the S_N method, an integral of general functions over $\mathcal S$ is represented as a weighted summation, that is,

$$\int_{\mathcal{S}} \Psi_{g} d\Omega' = \sum_{d=1}^{N_d} w_d \Psi_{g,d}.$$

It is straightforward to apply the technique to (2.7). Take the collision term as an example, we have

$$(2.8) \qquad (\mathbf{L}_{2}\mathbf{\Psi}^{*},\mathbf{\Psi}) = \sum_{g=1}^{G} \int_{\mathcal{S}} d\Omega \left(\Sigma_{\mathsf{t},g} \mathbf{\Psi}_{g}^{*}, \mathbf{\Psi}_{g} \right)_{\mathcal{D}} = \sum_{g=1}^{G} \sum_{d=1}^{N_{d}} w_{d} \left(\Sigma_{\mathsf{t},g} \mathbf{\Psi}_{g,d}^{*}, \mathbf{\Psi}_{g,d} \right)_{\mathcal{D}},$$

where $(\cdot,\cdot)_{\mathcal{D}}$ denotes that the integral is taken over \mathcal{D} only. For the spatial discretization, the first-order Lagrange finite element is applied to $(\cdot,\cdot)_{\mathcal{D}}$. For more details on the angular and spatial discretization of the neutron transport equations used in this work, please see [33]. After the angular and spatial discretization, a large eigenvalue system with the dense coupling block matrices in the energy and angle is produced. The potential dense matrix in energy is generated because a high energy neutron can be scattered down to a low energy group (down-scattering) and a low energy neutron can be also scattered up to a high energy group (up-scattering). The equation is fully coupled in the angle. We will introduce a scalable eigenvalue solver in next Section to handle the large system of eigenvalue equations.

3. Scalable parallel algorithm framework. In this Section, we describe the parallel algorithm framework consisting of the Newton method for calculating the nonlinear system of equations, the Krylov subspace method for solving the Jacobian system and the Schwarz preconditioner for accelerating the linear solver.

The corresponding agebraic system of equations for (2.7) reads as

(3.1)
$$\mathcal{A}\Psi = \frac{1}{k}\mathcal{B}\Psi,$$

where Ψ is also used to represent the solution vector that corresponds to the nodal values of the neutron flux at the mesh vertices, \mathcal{A} is the corresponding matrix of \mathbb{A} , and \mathcal{B} is the corresponding matrix of \mathbb{f} . Note that the matrices \mathcal{A} and \mathcal{B} are not necessary to be formed explicitly, and we will have a detailed discussion on this shortly. The simplest algorithm for the eigenvalue calculation of (3.1) is the inverse power iteration, shown in Alg. 3.1, that works well only when the ratio of the minimum eigenvalue to the second smallest eigenvalue is sufficient small, but it converges slow or even fails to converge when the ratio is close to "1". The difficulty is overcome by a

Algorithm 3.1 Inverse power iteration. " \leftarrow " represents that the corresponding vector is scaled in place. max_e is the maximum number of inverse power iterations. tol_{Ψ} and tol_k are relative tolerances for the eigenvalue and the eigenvector, respectively.

```
1: Initialize \Psi_0

2: Compute eigenvalue: k_0 = \|\mathcal{B}\Psi_0\|

3: Scale \mathcal{B}\Psi_0 \leftarrow \frac{1}{k_0}\mathcal{B}\Psi_0

4: for n = 0,..., \max_e do

5: \mathcal{A}\Psi_{n+1} = \mathcal{B}\Psi_n

6: k_{n+1} = \|\mathcal{B}\Psi_{n+1}\|

7: Scale \mathcal{B}\Psi_{n+1} \leftarrow \frac{1}{k_{n+1}}\mathcal{B}\Psi_{n+1}

8: if \frac{\|\Psi_{n+1} - \Psi_n\|}{\|\Psi_n\|} < \operatorname{tol}_{\Psi} and \frac{|k_{n+1} - k_n|}{|k_n|} < \operatorname{tol}_k then

9: Break

10: end if

11: end for

12: Output k_{n+1} and \Psi_{n+1}
```

Newton method that accelerates the convergence. To take the advantage of Newton, lines 5 and 6 of Alg. 3.1 are rewritten as follows:

(3.2)
$$\mathcal{F}(\mathbf{\Psi}) = \mathcal{A}\mathbf{\Psi} - \frac{1}{\|\mathcal{B}\mathbf{\Psi}\|}\mathcal{B}\mathbf{\Psi}.$$

And then an inexact Newton is applied to (3.2). More precisely, for a given Ψ_n , the new solution is updated as follows:

$$\mathbf{\Psi}_{n+1} = \mathbf{\Psi}_n + \bar{\mathbf{\Psi}}_n.$$

Here $\bar{\Psi}_n$ is the Newton update direction obtained by solving the following Jacobian system of equations

(3.4)
$$\mathcal{J}(\mathbf{\Psi}_n)\bar{\mathbf{\Psi}}_n = -\mathcal{F}(\mathbf{\Psi}_n),$$

where $\mathcal{J}(\Psi_n)$ is the Jacobian matrix at Ψ_n , and $\mathcal{F}(\Psi_n)$ is the nonlinear function residual evaluated at Ψ_n . To save the memory, $\mathcal{J}(\Psi_n)$ is not exceptibly formed, instead, it is carried out in a matrix-free manner. The corresponding Newton is referred to as "Jacobian-free Newton" method [11]. That is, a matrix-vector product, $\mathcal{J}(\Psi_n)\bar{\Psi}_n$, is approximated by

$$\mathcal{J}(\mathbf{\Psi}_n)\mathbf{\tilde{\Psi}}_n = \frac{\mathcal{F}(\mathbf{\Psi}_n + \delta\mathbf{\tilde{\Psi}}_n) - \mathcal{F}(\mathbf{\Psi}_n)}{\delta},$$

where δ is a small permutation that is a square root of the machine epsilon in this paper. (3.4) is solved using an iterative method such as GMRES [24], and a preconditioner is required to construct a scalable and efficient parallel solver. Let us rewrite (3.4) as a preconditioned form

$$\mathcal{J}\mathcal{P}^{-1}\mathcal{P}\bar{\Psi} = -\mathcal{F},$$

where \mathcal{P} is the preconditioning matrix that is often an approximation to \mathcal{J} , and \mathcal{P}^{-1} is a preconditioning process. The Jacobian \mathcal{J} is carried out in a matrix-free manner since it has dense diagonal blocks since all groups and all directions are coupled through the fission term and the scattering term. The preconditioning matrix \mathcal{P} is formed explicitly by only taking into consideration the first three terms of (2.7) since they form a SPD matrix that can be calculated using the multilevel method with algebraic coarse spaces. In fact, the angular fluxes in the energy and angle are independent in the first three terms of (2.7). If the variables were ordered group-by-group and direction-by-direction, \mathcal{P} is written as

$$\mathcal{P} = \begin{bmatrix} \mathcal{P}_{0,0} & & & \\ & \mathcal{P}_{1,1} & & \\ & & \ddots & \\ & & & \mathcal{P}_{G,G} \end{bmatrix},$$

where $P_{g,g}$ is a block diagonal matrix for the gth energy group expressed as

(3.7)
$$\mathcal{P}_{g,g} = \begin{bmatrix} \mathcal{P}_{g,g}^{(0,0)} & & & & \\ & \mathcal{P}_{g,g}^{(1,1)} & & & & \\ & & \ddots & & & \\ & & & \mathcal{P}_{g,g}^{(N_d,N_d)} \end{bmatrix}.$$

Here G is the number of energy groups, and N_d is the number of angular directions per energy group. $\mathcal{P}_{g,g'}$ represents the coupling matrix between groups g and g'. If the scattering and the fission terms were taken into account, \mathcal{P} would be a fully coupled matrix instead of the diagonal matrix shown in (3.6), that is, $\mathcal{P}_{g,g'} \neq 0$ when $g \neq g'$. $\mathcal{P}_{g,g}^{(d,d')}$ represents the coupling matrix between angular directions d and d' in the gth group. Similarly, if the fission term and the scattering term were considered in the preconditioning matrix, $\mathcal{P}_{g,g}^{(d,d')}$ would be a fully coupled dense matrix, that is, $\mathcal{P}_{g,g}^{(d,d')} \neq 0$ when $d \neq d'$. For the given group g and direction d, $\mathcal{P}_{g,g}^{(d,d)}$ is a large sparse matrix obtained from the spatial discretization. It is easy to note that the block structure in (3.6) corresponds to the multigroup approximation, and that in (3.7) corresponds to the angular discretization.

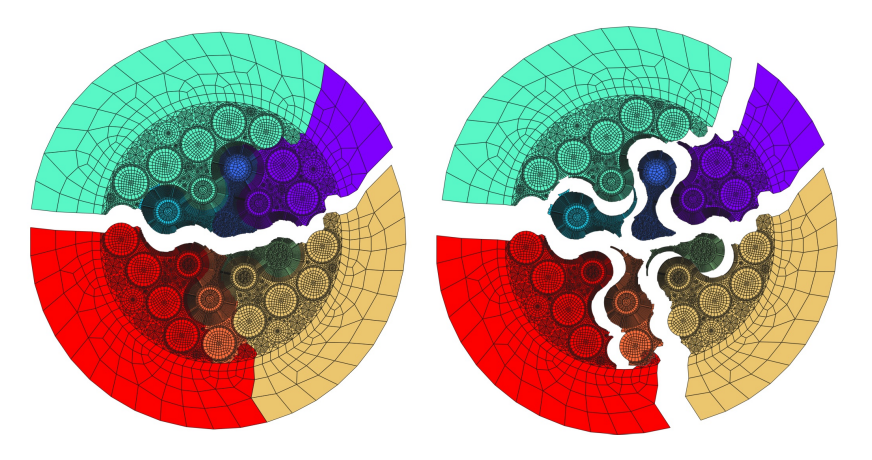


FIG. 2. Hierarchical partitioning. A mesh is paritioned into 2 "big" submeshes shown in the left, and then each "big" submesh is further into 4 small submeshes. We finally have 8 submeshes.

Generally speaking, a preconditioning procedure is designed to find the solution of the following residual equations,

$$(3.8) \mathcal{P}e = r,$$

where *r* is the residual vector from the outer solver (GMRES). To carry out the simulation in parallel, the mesh \mathcal{D}_h , corresponding to a triangulation of \mathcal{D} , is partitioned into np (np is the number of processor cores) submeshes $\mathcal{D}_{h,i}$, i = 1, 2, ..., np. This is accomplished by a hierarchical partitioning method since most existing partitioners such as ParMETIS [9] do not work well when the number of processor cores is close to or more than 10,000. The basic idea of the hierarchical partitioning is to apply an existing partitioner such as ParMETIS or PT-Scotch [5] twice. The computational mesh \mathcal{D}_h is first partitioned into np_1 "big" submeshes (np_1 often is the number of compute nodes), and each "big" submesh is further divided into np2 (np2 is the number of processor cores per compute node) small submeshes. A 2D example with assuming that each compute node has 4 processor cores is shown in Fig. 2, where the mesh is partitioned into 2 "big" submeshes, and then each "big" submesh is further divided into 4 small submeshes, and finally we have 8 small submeshes in total. Note that the hierarchical partitioning works for 3D meshes, and the 2D example is shown for the demonstration. Using the hierarchal partitioning method, we are able to not only produce a large number of submeshes, but also minimize the offnode communication since np_2 small submeshes on a compute node are physically connected and the communication between them is cheap. Interested readers are referred to our previous works [13, 18] for more details of the hierarchical partitioning. Let us denote the submatrix and the subvectors associated with a submesh $\mathcal{D}_{h,i}$ as \mathcal{P}_i , e_i and r_i , respectively. We define a restriction operator, R_i , that restricts a global vector r to a nonoverlapping submesh, that is, $r_i = R_i r$. With those notations, the one-level nonoverlapping Schwarz preconditioner is expressed as

(3.9)
$$\mathcal{P}_{one}^{-1} = \sum_{i=1}^{np} R_i^T \mathcal{P}_i^{-1} R_i, \ \mathcal{P}_i = R_i \mathcal{P} R_i^T$$

where \mathcal{P}_i^{-1} is a subdomain solver that is a successive over-relaxation (SOR) algorithm in this paper. The subdomain restriction R_i does not extract any overlapping

values. The overlapping version of (3.9) has been successfully employed in our previous works [13, 14, 16, 17] for elasticity equations, incompressible flows and fluid-structure interactions. Interested readers are referred to [27, 29] for more details on the Schwraz methods. After many experiments, we find that the nonoverlapping Schwarz preconditioner is able to maintain a strong scalability for the targeting applications when it is equipped with the subspace-based coarse spaces to be introduced shortly, and meanwhile the nonoverlapping Schwarz preconditioner uses less memory and communication compared with the overlapping version since no ghosting matrix entries need to be stored and exchanged. Coarse spaces need to be investigated for \mathcal{P}_{one}^{-1} to form its multilevel version when the number of processor cores is large, the materials are heterogeneous and the computational domain is complex. Let us denote L spaces as $\mathcal{D}_h^{(1)}, \mathcal{D}_h^{(2)}, ..., \mathcal{D}_h^{(L)}$, and the associated operators as $\mathcal{P}^{(1)}, \mathcal{P}^{(2)}, ..., \mathcal{P}^{(L)}$. Here $\mathcal{D}_h^{(1)} = \mathcal{D}_h$ and $\mathcal{P}^{(1)} = \mathcal{P}$. The interpolation operator from $\mathcal{D}_h^{(l+1)}$ to $\mathcal{D}_h^{(l)}$ is denoted as I_{l+1}^l , and the corresponding restriction operator from $\mathcal{D}_h^{(l)}$ to $\mathcal{D}_h^{(l+1)}$ is $(I_{l+1}^l)^T$. A multilevel additive Schwarz preconditioner (abbreviated as "MASM") is summarized as Alg. 3.2. The fundamental motivation behind

```
Algorithm 3.2 MASM(\mathcal{P}^{(l)}, e^{(l)}, r^{(l)})
```

```
1: if l = L then
          Solve \mathcal{P}^{(L)}e^{(L)}=r^{(L)} with a redundant direct solver on each compute node
 2:
 3: else
          Pre-solve \mathcal{P}^{(l)}e^{(l)} = r^{(l)} using an iterative solver preconditioned by (\mathcal{P}_{one}^{(l)})^{-1}
 4:
          Set \bar{r}^{(l)} = r^{(l)} - \mathcal{P}^{(l)}e^{(l)}
 5:
         Apply the restriction: \bar{r}^{(l+1)} = (I_{l+1}^l)^T \bar{r}^{(l)}
 6:
         z^{(l+1)} = \text{MASM}(\mathcal{P}^{(l+1)}, z^{(l+1)}, \bar{r}^{(l+1)})
 7:
         Apply the interpolation: z^{(l)} = I_{l+1}^{l} z^{(l+1)}
          Correct the solution: e^{(l)} = e^{(l)} + z^{(l)}
          Post-solve \mathcal{P}^{(l)}e^{(l)} = r^{(l)} using an iterative solver preconditioned by (\mathcal{P}_{one}^{(l)})^{-1}
10:
11: end if
12: Return e^{(l)}
```

Alg. 3.2 is that the high frequency mode of the solution is efficiently resolved using an iterative method together with the preconditioner \mathcal{P}_{one}^{-1} , and then the remaining low high frequencies will be handled in the coarse levels. The performance of Alg. 3.2 is largely affected by how to construct coarse spaces and their associated interpolations. Generally speaking, there are two ways to construct a set of coarse spaces. The first approach is to geometrically coarsen the fine mesh \mathcal{D}_h to generate coarse meshes, which has been shown to be powerful in our previous works [13] for elasticity problems and [12, 14, 15] for fluid-structure interactions. However, the geometry of the targeting application is complex so that it is nontrivial to setup a geometric mesh coarsening algorithm. The second one is to construct coarse spaces without querying any mesh information, instead, the coarse spaces and their interpolations are derived based on the matrix information only. The second approach has been successfully applied for different applications [7, 32, 34]. However, it is well known that the setup phase of the algebraic-version preconditioner is not strongly scalable in terms of the compute time since the matrix coarsening and the interpolation construction are expensive [34]. Fortunately, the overall algorithm can be still scalable if

the preconditioner setup phase accounts for a reasonably small portion of the total compute time. We will introduce such a new subspace-based coarsening algorithm that the preconditioner setup time is significantly reduced and the overall algorithm is able to maintain a good scalability with more than 10,000 processor cores. We will give a detailed description of the proposed coarsening algorithm in next Section.

- **4. Coarse spaces.** In this section, we discuss a coarse space construction for Alg. 3.2. First, a matrix coarsening algorithm based on subspace is introduced, where the "grid" point selection is accomplished using a submatrix instead of the global matrix. A subinterpolation is constructed based on the splitting of the coarse points and the fine points, and the global interpolation is built from the subinterpolation.
- **4.1. Matrix coarsening based on subspace.** According to (3.6) and (3.7), it is easily found that \mathcal{P} is a block diagonal matrix and each block corresponds to the spatial discretization of (2.2) for a given energy group and angular direction. Furthermore, there is no coupling between a block and the other blocks since we ignore the scattering and the fission terms in the preconditioning matrix. The individual matrix blocks are similar to each other in the sense that they correspond to the same continuous operators and share the same computational mesh \mathcal{D}_h . The differences between them come from different materials (i.e. cross sections) being used by different energy groups. Our motivation here is to coarsen a block of \mathcal{P} instead of the entire matrix to generate subinterpolations, and then the subinterpolations are expanded to covered the entire space by defining an expanding operator. The benefit of this approach is potentially save a lot of the setup time and also the memory usage since the coarsening phase operates on a much smaller data set. Let us define a restriction $R_{s,i}$ that extracts the corresponding components from the entire vector r for a given angular direction and energy group to form a subspace vector $r_{s,i}$, $i = 1, 2, ..., G \times N_d$, that is,

$$r_{s,i} = R_{s,i}r \equiv \left(\begin{array}{cc} \mathbf{I} & \mathbf{0} \end{array} \right) \left(\begin{array}{c} r_{s,i} \\ r/r_{s,i} \end{array} \right),$$

where "/" denotes the components in r but not in $r_{s,i}$. The choice of energy groups and angular directions is arbitrary in this paper, and we use the first energy group and angular direction, that is, i=1. Without any confusion, we drop the second subscript of $r_{s,1}$ and $R_{s,1}$, and denote them as r_s and R_s , respectively, for the simplicity of notations. With these notations, a subspace preconditioning matrix (for the first energy group and angular direction) is formed as

$$\mathcal{P}_s = R_s \mathcal{P} R_s^T.$$

Here \mathcal{P}_s can be coarsened using one of the existing matrix coarsening algorithms. We use a hybrid method of the Ruge-Stüben (RS) coarsening [28] and the Cleary-Luby-Jones-Plassman (CLJP) coarsening method [32]. For completeness, we briefly describe these methods here, and interested readers are referred to [22, 23, 34] for more details. Before starting a coarsening process, a "strength" matrix (graph), $\mathcal{G} = (V, E)$, need to be constructed from \mathcal{P}_s since not all coefficients are equally important to determine the coarse spaces (grids) and we should consider the important coefficients only. Here V is a set of all points in \mathcal{P}_s , that is, $V = \{v_i\}$, and the size of V is the number of rows of \mathcal{P}_s . E is a set of the corresponding edges, that is, $E = \{\tilde{e}_{ij}\}$. An edge \tilde{e}_{ij} is formed when v_i strongly depends on v_j or v_j strongly influences v_i according to the following formula

$$(4.2) -p_{ij} \geq \theta \max_{k \neq i} (-p_{ik}),$$

where p_{ij} is an entity of \mathcal{P}_s , and θ is the strength threshold that sometimes has an important impact on the overall algorithm performance because it changes the matrix complexities, the stencil sizes, and the solver convergence rate. A coarsening algorithm tries to split V into either coarse points (C-point), denoted as C, which will be taken into the next level, or fine points (F-points), denoted as F, which will be interpolated by C-points.

The RS coarsening algorithm (also referred to as "classical" coarsening in some literatures) has two targets:

A1 For each point v_j that strongly influences an F-point v_i , v_j is either a C-point or it shares a common C-point v_k with v_i

A2 C should be a maximal independent set

"A1" is designed to insure the quality of interpolation, while "A2" controls the size of the coarse space and the complexity of the operator. In practice, it is hardly to satisfy both conditions at the same time. The RS coarsening tries to meet A1 while uses A2 as a guideline and it is carried out in two passes. In the first pass, each point v_i is assigned by a measure m_i that equals the number of the points strongly influenced by v_i , and the point with the maximum measure is selected as C-point, v_c . All the points strongly influenced by v_c are chosen as new F-points, $\{v_f\}$. For each unmarked point that strongly influences any point in $\{v_f\}$, its measure is increased by the number of F-points it influences. This procedure is repeated until all points are chosen as either C-points or F-points. In the second pass, the algorithm checks every strong F-F connection if two F-points have a common C-point. If there is no a common C-point, and then one of the two F-points is chosen as a C-point. The approach is summarized in Alg. 4.1. It is easily seen that the RS algorithm is inherently sequential. A completely parallel coarsening approach is suggested in [6, 32]. It is based on a parallel maximal independent set (MIS) algorithm as described in [22], and is often denoted as "CLJP" (Cleary-Luby-Jones-Plassman) in other literatures. The CLJP coarsening algorithm starts with adding a measure m_i for each point $v_i \in V$ just like the RS coarsening algorithm. Each m_i is added by a small random value between 0 and 1 so that the points are distinctive even if the original measures are the same. It is now possible to find a local maximum of all the point measures independently in parallel. A point v_i with the local maximal measure is selected as a C-point, and the measures of the neighboring points strongly influenced by v_i are decreased by 1. Furthermore, for all the points $\{v_i\}$ that strongly depend on v_i , remove their connections to v_i . Examine all the points $\{v_k\}$ that depend on $v_i \in \{v_i\}$ whether or not they also depend on v_i . If v_i is a common C-point of v_k and v_i , remove the connection from v_k to v_i and decrease the measure of v_i by 1. If the measure of $v_i \in \{v_i\}$ is smaller than 1, it is chosen as a F-point. This procedure is repeated until all points are selected as either C-points or F-points. The algorithm is summarized in Alg. 4.2. While this approach works well for many applications, another option that has been shown to be even better is the combination of the RS coarsening and the CIJP coarsening [32]. This coarsening starts with Alg. 4.1 of which the first pass is applied to the local graph independently in parallel. The interior C-points and F-points generated in Alg. 4.1 are used as an initial for Alg. 4.2. The resulting coarsening, which satisfies A1, fills the boundaries with further C-points and possibly adds a few in the interior of the subdomains. For convenience, the algorithm is denoted as "HCIJP" (hybrid CIJP coarsening, and it is also referred to as "Falgout" in [32]) and shown in Alg. 4.3. While these approach work well for many applications, they sometimes lead to high complexities. There are some options that can be used to resolve these

Algorithm 4.1 Subspace based RS coarsening

```
1: Input: \mathcal{P}
                                                                      2: Extract a submatrix: \mathcal{P}_s = R_s \mathcal{P} R_s^T
3: Construct a strength matrix of \mathcal{P}_s, \mathcal{G} = (V, E), according to (4.2)
4: Compute measures \{m_i\} for all points in V = \{v_i\}
5: Set C = \emptyset, F = \emptyset
6: while V \neq \emptyset do
                                                                                        ⊳ Pass 1
       Find a point v \in V that has the maximum measure
8:
       C = C + v
9:
       Find the neighbors of v (denoted as V_n \subset V) that strongly depend on v
       V = V - v
10:
       F = F + V_n
11:
       for v_n \in V_n do
12:
13:
           Find the neighbors of v_n (denoted as V_{nn} \subset V ) that strongly influence v_n
           for v_{nn} \in V_{nn} do
14:
15:
               m_{nn}=m_{nn}+1
           end for
16:
       end for
17:
       V = V - V_n
18:
19: end while
20: for v_i \in F do
                                                                                        ⊳ Pass 2
       Find the neighbors of v_i (denoted as F_n \subset F) that strongly influence v_i
21:
22:
       for v_n \in F_n do
           if v_n and v_i do not share a common C-point then
23:
               F = F - v_n
24:
               C = C + v_n
25.
26:
           end if
       end for
27:
28: end for
29: Output: C, F
```

issues. The first one is to loose A1 as: A F-point should strongly depends on at least one C-point. This approach often decreases the complexity, but the complexity can be still high and require more memory than desired. This is further improved by an aggressive coarsening algorithm that is most efficiently implemented by applying the coarsening algorithms twice, The resulting aggressive coarsening algorithm is briefly described in Alg. 4.4.

4.2. Interpolation construction based on subspace. With a splitting (C, F), we consider the construction of interpolation. For a given F-point v_i , its interpolation takes the form as follows:

$$e_i = \sum_{j \in C_i} w_{ij} e_j,$$

where C_i is the coarse interpolatory set of v_i , and w_{ij} is an interpolation weight determing the contribution of e_j to e_i . We assume that an algebraically smooth error corresponds to a small residual, that is, $\mathcal{P}_s e \approx 0$ when e is algebraically smooth. Let $V_{n,i}$ be the neighboring points of v_i , which strongly or weakly influence v_i , and then

Algorithm 4.2 Subspace based CIJP coarsening

```
1: Input: \mathcal{P}
                                                                       2: Extract a submatrix: \mathcal{P}_s = R_s \mathcal{P} R_s^T
 3: Construct a strength matrix of \mathcal{P}_s, \mathcal{G} = (V, E), according to (4.2)
 4: Compute measure \{m_i\} for all point in V = \{v_i\}
 5: Set C = \emptyset, and F = \emptyset
 6: Add a random between 0 and 1 to each m_i \in \{m_i\}
                                                                                        ⊳ Pass 1
   while V \neq \emptyset do
        Find a point v \in V that has the local maximum measure
 8:
 9:
        C = C + v
       Find the neighbors of v (denoted as V_n \subset V) that strongly depend on v
10:
        for v_n \in V_n do
11:
            m_n = m_n - 1
12:
13:
            Find the neighbors of v_n (denoted as V_{nn} \subset V ) that strongly depends on
   v_n
            for v_{nn} \in V_{nn} do
14:
               if v_{nn} also depends on v then
15:
                   m_{nn} = m_{nn} - 1
16:
               end if
17:
18:
            end for
        end for
19:
       for v_n \in V_n do
20:
           if m_n < 1 then
21:
               F = F + v_n
22:
23:
               V = V - v_n
            end if
24:
25:
        end for
        V = V - v
26:
27: end while
28: Output: C, F
```

Algorithm 4.3 Subspace based HCIJP coarsening

```
1: Input: \mathcal{P} \triangleright Submatrix extraction

2: Extract a submatrix: \mathcal{P}_s = R_s \mathcal{P} R_s^T

3: Construct a strength matrix of \mathcal{P}_s, \mathcal{G} = (V, E), according to (4.2)

4: Compute measure \{m_i\} for all point in V = \{v_i\}

5: Set C = \emptyset, and F = \emptyset

6: Apply the first pass of Alg. 4.1

7: Apply the first pass of Alg. 4.2

8: Output: C, F
```

the *i*th equation of $P_s e \approx 0$ reads as

$$(4.3) p_{ii}e_i + \sum_{j \in V_{n,i}} p_{ij}e_j \approx 0.$$

Here $V_{n,i}$ comprises three sets: C_i (coarse neighbors), F_i^w (weakly influencing neighbors) and F_i^s (strongly influencing neighbors). A "classical" interpolation, as de-

Algorithm 4.4 Subspace based aggressive HCIJP coarsening

1: Input: \mathcal{P}

- 2: Extract a submatrix: $\mathcal{P}_s = R_s \mathcal{P} R_s^T$
- 3: Construct a strength matrix of \mathcal{P}_s , $\mathcal{G} = (V, E)$, according to (4.2)
- 4: Compute measure $\{m_i\}$ for all point in $V = \{v_i\}$
- 5: Set $C = \emptyset$, and $F = \emptyset$
- 6: Apply the first pass of Alg. 4.3 to \mathcal{G}
- 7: Apply the first pass of Alg. 4.3 to C
- 8: Output: C, F

scribed in [23], is constructed as

(4.4)
$$w_{ij} = -\frac{1}{p_{ii} + \sum_{k \in F_i^w p_{ik}} (p_{ij} + \sum_{k \in F_i^s} \frac{p_{ik} p_{kj}}{\sum_{m \in C_i p_{km}}}).$$

Eq. (4.4) is easy to implement in parallel since it only involves immediate neighbors and only requires one layer of the ghosting points. This method is invalid if A1 is not met. Another interpolation scheme, often referred as "direction interpolation", which only needs immediate neighbors and can be used when A1 is violated, is expressed as

(4.5)
$$w_{ij} = -\frac{p_{ij}}{p_{ii}} \left(\frac{\sum_{k \in V_{n,i}} p_{ik}}{\sum_{l \in C_i} p_{il}} \right).$$

If an aggressive coarsening scheme such as Alg. 4.4 is adopted, it is necessary to use a long range interpolation, such as a "multipass interpolation" as described in [28], in order to achieve a reasonable convergence. The "multipass" interpolation scheme starts with computing interpolating weights using (4.5) for the F-points immediately influenced by at least one C-point. In the second pass, for each F-point v_i that have not been interpolated yet, find its neighboring interpolated F-points v_j and then replace e_j with $\sum_{k \in C_j} w_{jk}e_k$ in Eq. (4.3). A direct interpolation is then applied to the modified equation. We would like to refer interested readers to [7] for more details on different interpolation approaches. Let us denote the subinterpolation constructed using the submatrix \mathcal{P}_s as $I_{s,2}^1$ from the second level to first level. And the full interpolation I_2^1 is expanded using the subinterpolation as follows

(4.6)
$$I_2^1 = \sum_{i=1}^{G \times N_d} (R_i^{(1)})^T I_{s,2}^1 R_i^{(2)}$$

where $R_i^{(l)}$ is the restriction operator defined on the lth level for the ith variable. The full coarse operator is computed using a Galerkin method

(4.7)
$$\mathcal{P}^{(2)} = (I_2^1)^T \mathcal{P}^{(1)} I_2^1.$$

With the full coarse operator in (4.7) and the full interpolation in (4.6), the corresponding version of Alg. 3.2 is denoted as "MASM_{sub}", while that equipped with the traditional coarse operators and interpolations is simply written as "MASM". Note that the description in this Section focuses on generating one interpolation and one coarse operator, and it is straightforward to apply the idea to generate a sequence of coarse spaces.

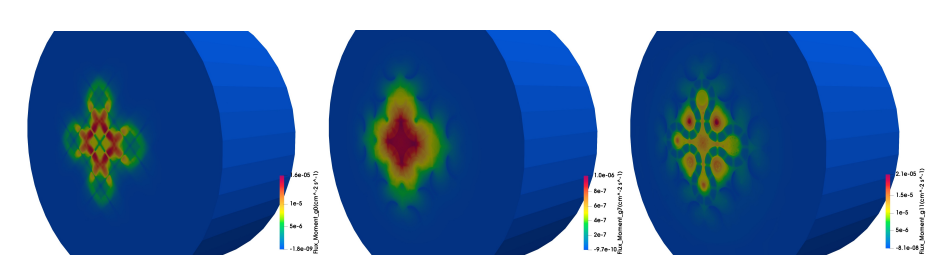


FIG. 3. Zero-order flux moments for 1st, 8th and 12th groups.

5. Numerical results. In this section, we report the algorithm's performance in terms of the compute time and the strong scalability for the eigenvalue calculation of the multigroup neutron transport equations for a realistic application, namely Advanced Test Reactor (ATR) that is located at the Reactor Technology Complex of the Idaho National Laboratory (INL) and is a 250-MW high flux test reactor. The ATR core, as shown in Fig 1, contains 40 fuel elements arranging in a serpentine annulus between and around nine flux traps. The algorithms are implemented based on PETSc [2] and hypre [20]. The numerical experiments are carried out on a supercomputer at INL, where each compute node has 36 processor cores (2.10 GHz per core) and the compute nodes are connected by a FDR InfiniBand Network of 56 Gbit/s. The problems are solved with an inexact Newton (3.3) together with GMRES preconditioned by Alg. 3.2, where 4 iterations of the inverse power, as shown in Alg. 3.1, is used to generate an initial guess for Newton. In the Newton eigenvalue solver, a relative tolerance of 10^{-6} is enfored for the nonlinear solver, and an inexact linear solver with a relative tolerance of 0.5 is adopted. In the inverse power, one iteration of Newton together with a linear solver with a relative tolerance of 10^{-2} is employed. The eigenvalue functions for 1st, 8th and 12th are shown in Fig 3. For convenience, let us define some notations that will be used in the rest of discussions. "np" represents the number of processor cores, "NI" is the total number of Newton iterations, "LI" denotes the total number of GMRES iterations, "Newton" is the total compute time spent on the nonlinear solvers and the inverse power iteration, "LSolver" is the compute time on the linear solver, "MF" is the compute time of the matrix-free operations, "PCSetup" is the compute time of the preconditioner setup, "PCApply" is the compute time of the preconditioner apply, "EFF" is the parallel efficiency, and "NR" is the ratio of the maximum number of mesh nodes to the minimum number of mesh nodes. "LSolver" is part of "Newton", and it consists of "MF" and the preconditioner. The preconditioner time is split into "PCSetup" and "PCApply".

5.1. Comparison with traditional MASM. We compare the proposed algorithm (denoted as "MASM_{sub}") with the traditional MASM. We use a mesh with 4,207,728 elements and 4,352,085 nodes, where, at each node, there are 96 unknowns consisting of 12 energy groups and 8 angular directions. That is, the angle is discretized by Level-Symmetric 2 with 8 angular directions. The resulting system of nonlinear equations with 417,800,160 unknowns is solved using 1,152, 2,304, 4,608, and 8,208 processor cores, respectively. The performance comparison with the traditional MASM is summarized in Table 1 and Fig. 4. The nonlinear eigenvalue solver consists of Jacobian evaluation, function evaluation, matrix-vector multiplication, preconditioner setup and preconditioner apply, and where most components except the preconditioner setup are mathematically scalable. As we discussed earlier, the preconditioner setup including the matrix coarsening and the interpolation construction

TABLE 1

Performance comparison with MASM for a problem with 417,800,160 unknowns. The resulting system of nonlinear equations with 417,800,160 unknowns is solved by an inexact Newton with MASM_{sub} and MASM on 1,152, 2,304, 4,608, and 8,208 processor cores, respectively.

пр	scheme	NI	LI	Newton	LSolver	MF	PCSetup	PCApply	EFF
1,152	MASM _{sub}	13	191	1855	1701	1418	26	290	100%
1,152	MASM	13	251	2640	2486	1900	162	476	
2,304	MASM _{sub}	13	193	989	908	749	21	154	93%
2,304	MASM	13	196	1277	1196	761	155	298	73%
4,608	MASM _{sub}	13	202	581	535	440	18	90	80%
4,608	MASM	13	194	985	939	426	199	328	47%
8,208	MASM _{sub}	14	216	404	372	294	22	66	64%
8,208	MASM	13	192	866	835	261	241	343	30%

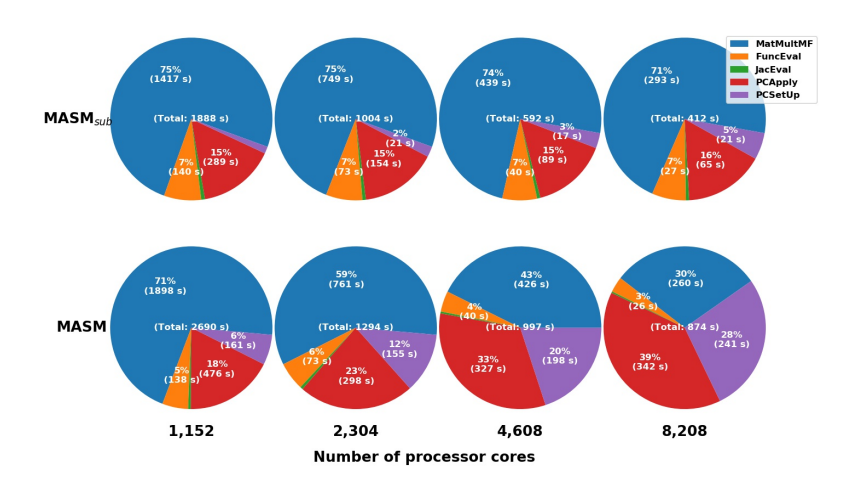


FIG. 4. Performance comparison with MASM. The figure shows the compute time spent on Jacobian evaluations ("JacEval"), function evaluations ("FuncEval"), matrix vector multiplications via matrix-free ("Mat-MultMF"), preconditioner setup ("PCSetUp") and preconditioner apply ("PCApply"), respectively.

is challenging to parallel, and its compute time sometimes increases significantly when we increase the number of processor cores, which deteriorates the overall algorithm. From Fig. 4, we observed that the preconditioner setup for the traditional MASM is not scalable, and the ratio of the preconditioner setup time to the total compute time is increased significantly when we increase the number of processor cores. The ratio is only 6% when the number of processor cores is 1, 152, but it jumps to 28% when we use 8,208 processor cores. For the preconditioner setup time, it is 161 s at 1,152 cores and increased to 261 s when 8,208 processor cores is used. In the traditional MASM, the precodnitioner setup not only is unscalable, but also takes a big chunk of the total compute time so that the overall algorithm performance is deteriorated and the parallel efficiency is reduced to 30% at 8,208 processor cores. On the other hand, the preconditioner setup of MASM_{sub} performs better since it accounts for only 3% (26 s) of the total compute time at 1,152 cores and it slightly increases to 6% (22 s) when we use 8, 208 processor cores. An interesting thing is that the preconditioner setup time of $MASM_{sub}$ does not increase much and stays close to a constant. That makes the overall algorithm scale much better, and the parallel efficiency is about 64% even when the number of processor cores is large, i.e., 8, 208.

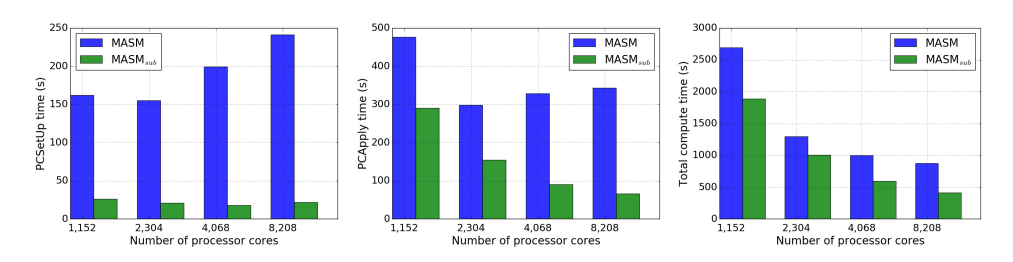


FIG. 5. The compute time comparison on different phases for the problem with 417,800,160 unknowns. Left: preconditioner setup time; middle: preconditioner apply time; right: total compute time.

The coarsening algorithm affects not only the preconditioner setup time but also the preconditioner apply time. In the traditional MASM, we observed that the preconditioner apply is not ideally scalable since while it accounts for 16% of the total compute time for 1, 152 processor cores, the ratio is increased to 39% at 8, 208 cores. The corresponding preconditioner apply time is 476 s for 1,152 processor cores, and it is decreased to 298 s by 37 s when we double the number of processor cores. Ideally, the preconditioner apply time should be reduced by 50% when the core count is doubled. The preconditioner apply of MASM_{sub} is scalable in the sense that the compute time is decreased from 289 s to 154 s by 47% when we double the number of processor cores from 1,152 to 2,304, and it is further decreased to 89 s when we use 4,608 processor cores. The traditional MASM does not preserve this property, and its preconditioner apply time is actually increased to 327 s from 298 s when the core count is doubled from 2,304 to 4,608. The coarsening algorithm based on subspace make MASM_{sub} scalable for the ATR simulation while the traditional MASM does not perform well. At 8,208 core, MASM_{sub} is twice faster than MASM. These behaviors can be observed from Table 1 as well, where the number of Newton iterations is similar for both MASM and MASM_{sub}, and the GMRES iteration of MASM_{sub} is slightly more than that of MASM at 4,608 and 8,208 cores. The impact of the slight increase of GMRES iteration is negligible since the preconditioner apply per iteration is scalable for MASM_{sub}. "LSolver" accounts for the most of the overall compute time, and the overall algorithm is scalable as long as the linear solver performs well. The peformance of the linear solver is almost completely determined by the preconditioner since "MF" is well-known to be scalable mathematically. In summary, the eigenvalue solver together with MASM is not scalable, while the MASM_{sub} equipped eigenvalue solver performs well since the setup phase of MASM_{sub} is optimized and the apply phase of MASM_{sub} scales well. The same performance comparison is observed in Fig. 5 as well, where the preconditioner setup of MASM_{sub} is almost 10 times faster than MASM for all processor counts. The preconditioner apply for MASM_{sub} is 2 or 3 times more efficient than MASM when the number of processor cores is small, and 5 times faster at 8,208 cores. Due to these behaviors, the overall algorithm based on MASM_{sub} is much better than that with MASM. Note that the total compute time in Fig. 4 is slightly more than that in Table 1 since it is calculated by summing up all the individual components that have some overlap.

To further verify the effectiveness of the proposed algorithm, we add more angular directions for each mesh node, which leads to 288 variables (24 angular directions \times 12 energy groups) one each mesh node. The same mesh as before is used, but the resulting system is much larger than the previous test, having 1,253,400,480 unknowns, since more angular directions are added for each mesh node. The numer-

TABLE 2

Performance comparison with MASM for a problem with 1,253,400,480 unknowns. The resulting system of nonlinear equations with 1,253,400,480 unknowns is solved by an inexact Newton with MASM $_{\rm sub}$ and MASM on 2,304, 4,608, 8,208, and 10,008 processor cores, respectively.

пр	scheme	NI	LI	Newton	LSolver	MF	PCSetup	PCApply	EFF
2,304	MASM _{sub}	13	191	2202	2027	1566	54	452	100%
2,304	MASM	12	147	2466	2302	1176	535	635	
4,608	$\begin{array}{c} {\rm MASM_{sub}} \\ {\rm MASM} \end{array}$	13	183	1199	1096	860	41	232	92%
4,608		12	139	1791	1694	641	496	589	61%
8,208	MASM _{sub}	13	183	828	763	552	68	176	75%
8,208	MASM	12	135	1474	1412	391	489	554	42%
10,008	MASM _{sub}	14	184	672	617	447	65	127	76%
10,008	MASM	12	134	1369	1317	322	480	531	37%

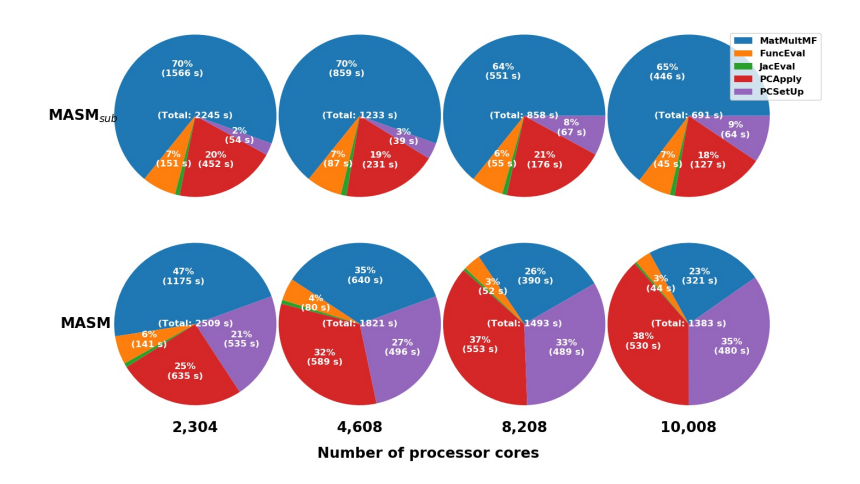


FIG. 6. Performance comparison with MASM for the problem with 1,253,400,480 unknowns. The figure shows the compute time spent on Jacobian evaluations ("JacEval"), function evaluations ("FuncEval"), matrix vector multiplications via matrix-free ("MatMultMF"), preconditioner setup ("PCSetUp") and preconditioner apply ("PCApply"), respectively.

ical results are summarized in Table 2, Fig. 6 and 7. In Table 2, it is easily seen that the number of Newton iterations stays close to a constant as we increase the number of processor cores from 2,304 to 10,008, and the number of GMRES iterations also keeps as a constant for both MASM and MASM $_{\rm sub}$. The number of GMRES iterations for MASM $_{\rm sub}$ is more than that obtained via MASM, but the performance of MASM $_{\rm sub}$ is not affected much and it is still much better than MASM. The overall algorithm based on MASM $_{\rm sub}$ has the parallel efficiency of 76% at 10,008 cores while that for MASM is only 37%. Similarly, from Fig. 6 and 7, we observed that the compute time of the preconditioner for MASM $_{\rm sub}$ is much smaller than that for MASM.

5.2. Node balance improvement. Typically, before a finite element simulation starts, a dual graph of mesh (where each graph vertex corresponds to a mesh element) is partitioned into *np* submeshes that have nearly equal number of elements. While the number of elements assigned to each processor core is nearly equivalent, some processor cores may have more mesh nodes since the shared mesh nodes along the processor boundaries are simply assigned to the cores with lower MPI rank. A scalable calculation requires to balance both mesh elements and mesh nodes. We

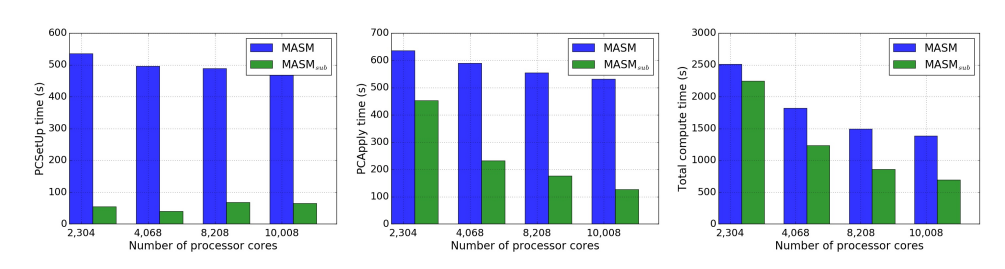


FIG. 7. The compute time comparison on different phases for the problem with 1,253,400,480 unknowns. Left: preconditioner setup time; middle: preconditioner apply time; right: total compute time.

TABLE 3
Mesh node assignment for the problems with 417,800,160 unknowns.

пр	scheme	NI	LI	Newton	LSolver	MF	PCSetup	PCApply	EFF
1,152 1,152	$\begin{array}{c} MASM_{sub} \\ MASM_{sub} + NB \end{array}$	13 13	191 199	1855 1821	1701 1674	1418 1407	26 26	290 270	100%
2,304	MASM _{sub}	13	193	989	908	749	21	154	92%
2,304	MASM _{sub} +NB	13	207	1005	928	769	19	158	91%
4,608	MASM _{sub}	13	202	581	535	440	18	90	78%
4,608	MASM _{sub} +NB	13	216	579	534	436	18	89	79%
8,208	MASM _{sub}	14	216	404	372	294	22	66	63%
8,208	MASM _{sub} +NB	14	217	379	348	272	21	62	67%

use a partition-based node assignment, as discussed in our previous work [18], to balance the overall calculation. The basic idea of the partition-based node assignment is that the processor boundary mesh is partitioned into two parts, and each part is assigned to a processor core who shares the processor boundary mesh with the other processor core. Interested readers are referred to [18] for more details. The same configuration as before is used, and the numerical results are shown in Table 3 and 4, and Fig. 8. From Table 3, we observed that the compute time for different components is further improved using the node assignment strategy. The improvement becomes more obvious when the number of variables for each mesh node is increased. In Table 4, the preconditioner setup time is significantly reduced, for example, it is reduced to $37 \ s$ from $65 \ s$ at 10,008 processor cores, which leads to the parallel efficiency increased from 76% from 83%. The same observation is found in Fig. 8 as well.

5.3. Aggressive coarsening. The numerical results shown earlier are obtained using 10 levels of aggressive coarsening. The aggressive coarsening, Alg. 4.4, is used to reduce the complexities of the operators and the interpolations. More levels are applied by the aggressive coarsening, and the complexities of the operators and the interpolations become lower, but at the same time the convergence may be deteriorated. In this test, different numbers of levels of aggressive coarsening are applied in MASM_{sub}, and the results are summarized in Table 5, where "Agg" denotes the number of levels of aggressive coarsening, and "Agg=0" corresponds to no aggressive coarsening. From Table 5, we observed that both Newton iteration and GMRES iteration do not change much when we apply different numbers of levels of the aggressive coarsening in MASM_{sub}. The preconditioner time including the setup and apply is reduced significantly when the number of levels of of aggressive coarsening is increased from 0 to 2, and then it slightly decreases when we increase "Agg"

TABLE 4	
Node assignment for the problem with with 1,253,400,480 unknow	vns.

пр	scheme	NI	LI	Newton	LSolver	MF	PCSetup	PCApply	EFF
2,304 2,304	$\begin{array}{c} {\rm MASM_{sub}} \\ {\rm MASM_{sub}} + {\rm NB} \end{array}$	13 13	191 191	2202 2203	2027 2018	1566 1575	54 49	452 433	100%
4,608	MASM _{sub}	13	183	1199	1096	860	41	232	92%
4,608	MASM _{sub} +NB	13	185	1093	1001	766	39	216	100%
8,208	MASM _{sub}	13	183	828	763	552	68	176	75%
8,208	MASM _{sub} +NB	13	189	732	670	511	37	138	84%
10,008	$\begin{array}{c} MASM_{sub} \\ MASM_{sub} + NB \end{array}$	13	184	672	617	447	65	127	76%
10,008		13	187	610	557	420	37	116	83%

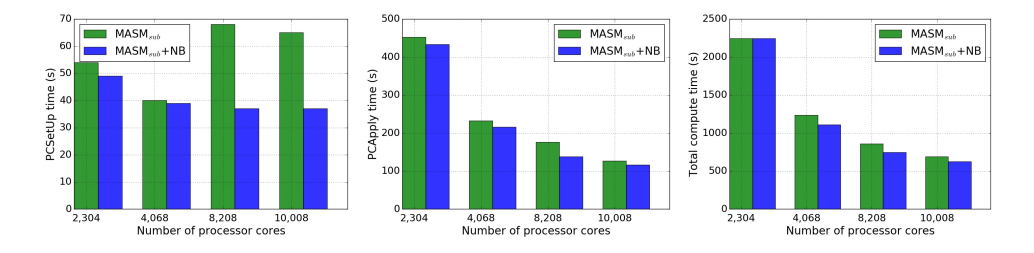


FIG. 8. The compute time comparison on different phases for the problem with 1,253,400,480 unknowns using a node balancing strategy. Left: preconditioner setup time; middle: preconditioner apply time; right: total compute time.

from 2, 4 to 10. For example, in 8,208-core case, the preconditioner apply time is decreased from 123 s to 87 s when "Agg" is increased from 0 to 2, and it is reduced to 70 s and 66 s when "Agg" is 4 and 8. Due to these factors, the corresponding parallel efficiency is increased from 53% to 64% when the number of levels of aggressive coarsening is increased from 0 to 10. It is the reason why we have used 10 levels of aggressive coarsening in our previous tests.

5.4. Strong scalability. In this test, we study the strong scalability using a "fine" mesh with 25,856,505 nodes and 26,298,300 elements. The resulting eigenvalue system of equations with 2,482,224,480 unknowns is solved by an inexact Newton preconditioned by MASM_{sub}. At the beginning of the strong scaling study, we also test the impact of the number of levels of aggressive coarsening on the overall algorithm for the "fine" mesh case. 4 and 10 levels of aggressive coarsening are tested, and the results are summarized in Table 6. The case with 10 levels of aggressive coarsening has slightly better results than that obtained with "Agg=4". We therefore use 10 levels of aggressive coarsening in the following scaling study. The numerical results are shown in Table 7. The performance of the node balancing strategy is also reported, and the corresponding algorithm is denoted as "MASM_{sub}+NB". Again, for MASM_{sub}, the numbers of Newton iterations and GMRES iterations stay as constants when we increase the number of processor cores, which indicates that the algorithm is mathematically scalable. The total compute time ("Newton") is decreased proportionally when we increase the number of processor cores from 4,608 to 10,008. For instance, the total compute is reduced from 2808 s to 2084 s, when we increase the number of processor cores from 4,608 to 6,048, and it further is reduced to 1707 s and 1423 s when the number of processor cores is 8,208 and 10,008. The preconditoner setup is not scalable, but it does not affect the overall performance much since it ac-

TABLE 5 Different number of aggressive coarsening levels for the problems with 417,800,160 unknowns. "Agg" denotes the number of aggressive coarsening levels.

np	Agg	NI	LI	Newton	LSolver	MF	PCSetup	PCApply	EFF
1,152	0	13	209	2242	2088	1853	55	509	100%
1,152	2	14	210	2068	1906	1570	33	347	_
1,152	4	13	206	2007	1853	1542	26	322	_
1,152	10	13	191	1855	1701	1418	26	290	-
2,304	0	13	208	1199	1118	820	45	278	77%
2,304	2	13	195	1027	945	758	25	178	90%
2,304	4	13	206	1059	978	801	20	174	88%
2,304	10	13	193	989	908	749	21	154	94%
4,608	0	13	206	677	632	457	34	160	68%
4,608	2	13	199	591	546	423	21	113	78%
4,608	4	13	210	606	558	449	18	104	80%
4,608	10	13	202	581	534	440	18	90	94%
8,208	0	14	217	490	457	302	46	123	53%
8,208	2	13	204	412	379	277	25	87	63%
8,208	4	13	200	385	355	273	21	70	68%
8,208	10	14	216	404	372	294	22	66	64%

Table 6
Different number of aggressive coarsening levels for the problem with 2,482,224,480 unknowns.

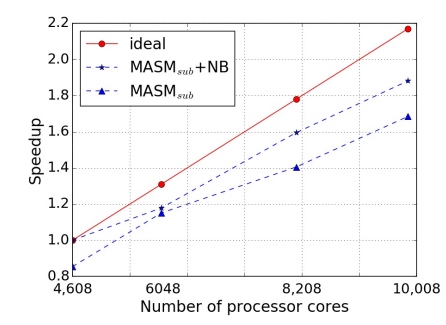
пр	Agg	NI	LI	Newton	LSolver	MF	PCSetup	PCApply	EFF
4,608	4	12	161	2596	2369	1853	114	457	100%
4,608	10	13	171	2808	2567	2002	131	511	
6,048	4	13	170	2125	1939	1499	95	391	93%
6,048	10	13	171	2084	1898	1510	84	352	95%
8,208	4	12	160	1749	1613	1134	150	404	83%
8,208	10	12	161	1707	1570	1139	142	364	85%
10,008	4	12	161	1459	1343	949	141	308	82%
10,008	10	12	160	1423	1307	951	138	274	84%

counts for only a small portion of the total compute time. A good parallel efficiency of 77% is achieved at 10,008. While the performance of MASM_{sub} is already good, it can be further enhanced by applying the node balancing strategy to make the overall distribution more balanced. In the odd rows of Table 7, the node balancing strategy is able to improve the overall algorithm performance, especially, the preconditioner setup time is significantly reduced. For example, at 8,208 cores, the compute time is reduced by 200 s when the node balancing strategy is used, most of the time reduction results from the improvement of the preconditioner setup. At 10,008 cores, the preconditioner setup time is reduced to 82 s from 138 s. The preconditioner apply also benefits from a more balanced workload, for example, the preconditioner apply time is reduced from 274 s to 208 s at 10,008 processor cores. We have almost-perfect parallel efficiencies when we use MASM_{sub}+NB. The parallel efficiency is as high as 87%, even when the number of processor cores is more than 10,000. The Schwarz preconditioner together with both the subspace-based coarsening and the partitionbased node balancing offers a highly scalable solver for the eigenvalue calculations for the targeting application. The corresponding parallel efficiency and speedup are plotted in Fig. 9.

6. Conclusions. A parallel Newton-Kyrlov-Schwarz method is studied for the numerical simulation of the multigroup neutron transport equations on 3D unstruc-

TABLE 7
Strong scalability with a "fine" mesh with 25,856,505 nodes, 26,298,300 elements, and 2,482,224,480 unknowns.

пр	Scheme	NI	LI	Newton	LSolver	MF	PCSetup	PCApply	NR	EFF
4,608	MASM _{sub} +NB	12	160	2398	2182	1743	94	396	1.8	100%
4,608	MASM _{sub}	13	171	2808	2567	2002	131	511	2.2	
6,048	MASM _{sub} +NB	13	176	2035	1858	1470	87	337	1.8	90%
6,048	MASM _{sub}	13	171	2084	1898	1510	84	352	2.7	89%
8,208	MASM _{sub} +NB	12	167	1504	1373	1081	76	244	2	90%
8,208	MASM _{sub}	12	161	1707	1570	1139	142	364	2.8	79%
10,008	MASM _{sub} +NB	13	168	1275	1160	896	82	208	2	87%
10,008	MASM _{sub}	12	160	1423	1307	951	138	274	2.9	77%



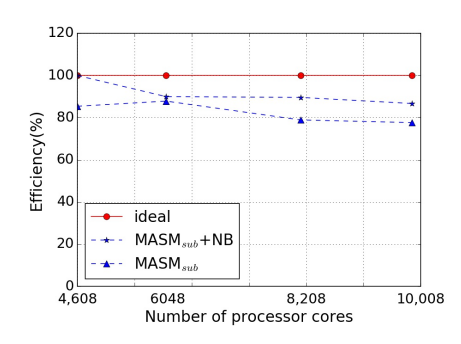


FIG. 9. Parallel efficiency and speedup for the problem with 2,482,224,480 unknowns. Left: speedup, right: parallel efficiency.

tured spatial meshes. A hierarchal partitioning is used to divide the computational domain into a large number of subdomains while the existing partitioners are from ideal. Two novel components including the subspace-based coarsening and the partition-based workload balancing are introduced and carefully studied. The total compute time using the subspace-based coarsening is halved compared with the traditional approach, and therefore the corresponding parallel efficiency is doubled to 76% when more than 10,000 processor cores are used. In addition, the partition-based workload balancing is able to assign a nearly equal amount of work to each processor core, and the parallel efficiency at 10,000 is further increased to 87%. The scalability of the overall algorithm is studied for a realistic application with 2,482,224,480 unknowns on a supercomputer with up to 10,008 processor cores.

While this paper focuses on the multilevel Schwarz preconditioner, other popular methods such as DSA [1] and NDA (nonlinear diffusion acceleration method) [25] will be explored in the future.

REFERENCES

- [1] R. E. Alcouffe, Diffusion synthetic acceleration methods for the diamond-differenced discrete-ordinates equations, Nuclear Science and Engineering, 64 (1977), pp. 344–355.
- [2] S. BALAY, S. ABHYANKAR, M. F. ADAMS, J. BROWN, P. BRUNE, K. BUSCHELMAN, L. DALCIN, A. DENER, V. EIJKHOUT, W. D. GROPP, D. KAUSHIK, M. G. KNEPLEY, D. A. MAY, L. C. McInnes, R. T. Mills, T. Munson, K. Rupp, P. Sanan, B. F. Smith, S. Zampini, H. Zhang, and H. Zhang, Petsc Users Manual, Tech. Report ANL-95/11 Revision 3.10, Argonne National Laboratory, 2018, http://www.mcs.anl.gov/petsc.
- [3] A. N. BROOKS AND T. J. HUGHES, Streamline upwind/Petrov-Galerkin formulations for convection domi-

- nated flows with particular emphasis on the incompressible Navier-Stokes equations, Computer Methods in Applied Mechanics and Engineering, 32 (1982), pp. 199–259.
- [4] B. CHANG, T. MANTEUFFEL, S. MCCORMICK, J. RUGE, AND B. SHEEHAN, Spatial multigrid for isotropic neutron transport, SIAM Journal on Scientific Computing, 29 (2007), pp. 1900–1917.
- [5] C. CHEVALIER AND F. PELLEGRINI, *PT-Scotch: A tool for efficient parallel graph ordering*, Parallel Computing, 34 (2008), pp. 318–331. https://doi.org/10.1016/j.parco.2007.12.001.
- [6] A. J. CLEARY, R. D. FALGOUT, AND J. E. JONES, Coarse-grid selection for parallel algebraic multigrid, in International Symposium on Solving Irregularly Structured Problems in Parallel, Springer, 1998, pp. 104–115.
- [7] H. DE STERCK, R. D. FALGOUT, J. W. NOLTING, AND U. M. YANG, Distance-two interpolation for parallel algebraic multigrid, Numerical Linear Algebra with Applications, 15 (2008), pp. 115–139.
- [8] P. GUÉRIN, A.-M. BAUDRON, AND J.-J. LAUTARD, Domain decomposition methods for core calculations using the MINOS solver, in Joint International Topical Meeting on Mathematics & Computation and super Computing in Nuclear Applications (M&C+SNA 2007), Monterey, CA, April 15-19, 2007.
- [9] G. KARYPIS AND K. SCHLOEGEL, PARMETIS: Parallel Graph Partitioning and Sparse Matrix Ordering Library, Tech. Report Version 4.0, University of Minnesota, 2013, http://glaros.dtc.umn.edu/ gkhome/metis/parmetis/overview.
- [10] D. KAUSHIK, M. SMITH, A. WOLLABER, B. SMITH, A. SIEGEL, AND W. S. YANG, Enabling highfidelity neutron transport simulations on petascale architectures, in Proceedings of the Conference on High Performance Computing Networking, Storage and Analysis, ACM, 2009, p. 67.
- [11] D. A. KNOLL AND D. E. KEYES, *Jacobian-free Newton-Krylov methods: a survey of approaches and applications*, Journal of Computational Physics, 193 (2004), pp. 357–397.
- [12] F. KONG, A Parallel Implicit Fluid-structure Interaction Solver with Isogeometric Coarse Spaces for 3D Unstructured Mesh Problems with Complex Geometry, PhD thesis, University of Colorado Boulder, 2016.
- [13] F. KONG AND X.-C. CAI, A highly scalable multilevel Schwarz method with boundary geometry preserving coarse spaces for 3D elasticity problems on domains with complex geometry, SIAM Journal on Scientific Computing, 38 (2016), pp. C73–C95.
- [14] F. KONG AND X.-C. CAI, A scalable nonlinear fluid–structure interaction solver based on a Schwarz preconditioner with isogeometric unstructured coarse spaces in 3D, Journal of Computational Physics, 340 (2017), pp. 498–518.
- [15] F. KONG AND X.-C. CAI, Scalability study of an implicit solver for coupled fluid-structure interaction problems on unstructured meshes in 3D, The International Journal of High Performance Computing Applications, 32 (2018), pp. 207–219.
- [16] F. KONG, V. KHEYFETS, E. FINOL, AND X.-C. CAI, An efficient parallel simulation of unsteady blood flows in patient-specific pulmonary artery, International Journal for Numerical Methods in Biomedical Engineering, 34 (2018), pp. 29–52.
- [17] F. KONG, V. KHEYFETS, E. FINOL, AND X.-C. CAI, Simulation of unsteady blood flows in a patient-specific compliant pulmonary artery with a highly parallel monolithically coupled fluid-structure interaction algorithm, arXiv preprint arXiv:1810.04289, (2018).
- [18] F. KONG, R. H. STOGNER, D. R. GASTON, J. W. PETERSON, C. J. PERMANN, A. E. SLAUGHTER, AND R. C. MARTINEAU, A general-purpose hierarchical mesh partitioning method with node balancing strategies for large-scale numerical simulations, in 2018 IEEE/ACM 9th Workshop on Latest Advances in Scalable Algorithms for Large-Scale Systems (ScalA), Dallas Texas, 11-16 November, 2018.
- [19] F. KONG, Y. WANG, S. SCHUNERT, J. W. PETERSON, C. J. PERMANN, D. ANDRŠ, AND R. C. MARTINEAU, A fully coupled two-level Schwarz preconditioner based on smoothed aggregation for the transient multigroup neutron diffusion equations, Numerical Linear Algebra with Applications, 25 (2018), pp. 21–62.
- [20] LAWRENCE LIVERMORE NATIONAL LABORATORY, hypre: High Performance Preconditioners. http://www.llnl.gov/CASC/hypre/.
- [21] E. E. LEWIS AND W. F. MILLER, Computational Methods of Neutron Transport, John Wiley and Sons Inc., New York, NY, 1984.
- [22] M. Luby, A simple parallel algorithm for the maximal independent set problem, SIAM Journal on Computing, 15 (1986), pp. 1036–1053.
- [23] J. W. RUGE AND K. STÜBEN, Algebraic multigrid, in Multigrid methods, SIAM, 1987, pp. 73–130.
- [24] Y. SAAD AND M. H. SCHULTZ, GMRES: A generalized minimal residual algorithm for solving nonsymmetric linear systems, SIAM Journal on Scientific and Statistical Computing, 7 (1986), pp. 856–869.
- [25] S. SCHUNERT, Y. WANG, F. GLEICHER, J. ORTENSI, B. BAKER, V. LABOURE, C. WANG, M. DE-HART, AND R. MARTINEAU, A flexible nonlinear diffusion acceleration method for the SN trans-

- port equations discretized with discontinuous finite elements, Journal of Computational Physics, 338 (2017), pp. 107–136.
- [26] R. SLAYBAUGH, T. M. EVANS, G. G. DAVIDSON, AND P. P. WILSON, Multigrid in energy preconditioner for Krylov solvers, Journal of Computational Physics, 242 (2013), pp. 405–419.
- [27] B. SMITH, P. BJORSTAD, W. D. GROPP, AND W. GROPP, Domain Decomposition: Parallel Multilevel Methods for Elliptic Partial Differential Equations, Cambridge university press, 2004.
- [28] K. STBEN, Algebraic multigrid (AMG): An Introduction with Applications, GMD-Forschungszentrum Informationstechnik, 1999.
- [29] A. TOSELLI AND O. WIDLUND, Domain Decomposition Methods-Algorithms and Theory, vol. 34, Springer Science & Business Media, 2006.
- [30] B. TURCKSIN, J. C. RAGUSA, AND J. E. MOREL, Angular multigrid preconditioner for Krylov-based solution techniques applied to the sn equations with highly forward-peaked scattering, Transport Theory and Statistical Physics, 41 (2012), pp. 1–22.
- [31] S. VAN CRIEKINGEN, F. NATAF, AND P. HAVÉ, parafish: A parallel FE-PN neutron transport solver based on domain decomposition, Annals of Nuclear Energy, 38 (2011), pp. 145–150.
- [32] U. M. Y. VAN EMDEN HENSON, BoomerAMG: a parallel algebraic multigrid solver and preconditioner, Applied Numerical Mathematics, 41 (2002), pp. 155–177.
- [33] Y. WANG, S. SCHUNERT, AND V. LABOURE, *Rattlesnake Theory Manual*, tech. report, Idaho National Laboratory (INL), Idaho Falls, ID (United States), 2018.
- [34] U. M. YANG, *Parallel algebraic multigrid methods-high performance preconditioners*, in Numerical Solution of Partial Differential Equations on Parallel Computers, Springer, 2006, pp. 209–236.
- [35] M. ZEYAO AND F. LIANXIANG, Parallel flux sweep algorithm for neutron transport on unstructured grid, The Journal of Supercomputing, 30 (2004), pp. 5–17.